Fluid Mechanics

Institution of MECHANICAL ENGINEERS

Journal of MECHANICAL ENGINEERING SCIENCE

Proc IMechE Part C:
J Mechanical Engineering Science
2023, Vol. 237(5) 1088–1105

DOI: 10.1177/09544062221126646
journals.sagepub.com/home/pic
SAGE

Numerical study of boundary stresses on Jeffery-Hamel flow subject to Soret/Dufour effects

Zaheer Asghar[1,2], Rai Sajjad Saif[3] and Abu Zar Ghaffari[4]

Abstract

We have mathematically modeled the problem of convective Jeffery-Hamel flow in the presence of thermo-diffusion and diffusion-thermo effects. The flow is considered to be the steady, incompressible and unidirectional by assuming the velocity only in radial direction. We have also modeled the boundary conditions representing the boundary stresses and assumed that these stresses apply only radially. Then we analyzed the effects of these stresses on the problem. The boundary stresses are defined through traction boundary conditions which are of Robin type. The flow is assumed in the domain $[-\alpha, \alpha]$ and the constant flow rate condition is applied instead of taking symmetry of the channel. The governing equations are nonlinear coupled partial differential equations. They become a system of nonlinear coupled ordinary differential equations by adopting suitable transformations. Therefore, they are handled numerically. For this purpose, we have developed a scheme using shooting method to solve nonlinear coupled differential equations representing the flow problem and shown the solution procedure via a flow chart. In order to obtain the numerical results, we have taken different values of parameters. Since we have considered the problem of Newtonian fluid, therefore, we considered the values Pr $= 0.7, 2.36, 7$ for air, carbon disulfide and water respectively at 25°C. Whereas the values of Schmidt number are considered as $Sc = 0.22, 0.62, 0.78$ for hydrogen, water vapor, and ammonia respectively at 25°C. The numerical solution is validated by comparing the results with those published in literature. The numerical results of present work show that there occurs no-slip for wedge angle of 2° by fixing the other parameters whereas slip is achieved in some other situations. It is noticed that the flow reversal occurs for convergent as well as divergent flow. All boundary layers are affected greatly due to presence of the boundary stresses and the hydrodynamic boundary layer that disappears in the absence of boundary stresses. The freedom in constraint of channel symmetry leads to the occurrence of symmetric as well as asymmetric flow. An interesting theoretical result of opposite behaviors of temperature and concentration profiles for convergent and divergent flows is observed in case of variation of all of the governing parameters. It is also noticed that the simultaneous increase of Soret number and decrease of Dufour number results in occurrence of opposite behavior of temperature and concentration profiles for divergent flow. However, it results in similar behavior of these profiles. The results show that the boundary layer completely disappears in the absence of boundary stresses.

Keywords

Traction boundary conditions, heat/mass transfer, shooting method, constant flow rate condition, boundary stresses

Date received: 25 January 2022; accepted: 29 July 2022

Introduction

The steady two dimensional flow of viscous fluid confined between nonparallel walls inclined at an arbitrary angle was first studied almost a century ago by Jeffery[1] and Hamel.[2] It is therefore termed as classical Jeffery-Hamel flow. These flows have many engineering and biological applications. Therefore, the governing equations of such flows have been extensively focused since the time of their introduction. For instance parametric effects on Jeffery-Hamel flow in context of hydrodynamic and magnetohydrodynamic Newtonian fluid were presented in.[3–13] In these

[1]Centre for Mathematical Sciences, Pakistan Institute of Engineering and Applied Sciences, Nilore Islamabad, Pakistan
[2]Department of Physics and Applied Mathematics, Pakistan Institute of Engineering and Applied Sciences, Nilore Islamabad, Pakistan
[3]Department of Humanities and Sciences, School of Electrical Engineering and Computer Science (SEECS), National University of Sciences and Technology (NUST), Islamabad, Pakistan
[4]Department of Mathematics, University of Education, Lahore, Attock Campus, Attock, Pakistan

Corresponding author:
Zaheer Asghar, Centre for Mathematical Sciences, Pakistan Institute of Engineering and Applied Sciences, Nilore, Islamabad, 45650, Pakistan; Department of Physics and Applied Mathematics, Pakistan Institute of Engineering and Applied Sciences, Nilore, Islamabad, 45650, Pakistan.
Email: zaheerasghar@pieas.edu.pk

investigations, Rosenhead[3] obtained solution in the form of elliptic functions and discussed various possible flow situations. The flow problem in a convergent and divergent channel in the presence of external magnetic field was discussed in Makinde and Mhone.[4] The spirit of the work was to obtain the semi-numerical solution of nonlinear problem using Hermite-Pade approximation. They discussed the reversal of flow and qualitative behavior of the problem. The spirit to obtain approximate analytical solution was also reflected in Esmaili et al.[5] but they used Adomian decomposition method. The focus of Domairry et al.[6] was to obtain analytical solution using Homotopy Analysis Method (HAM). They concluded that results were improved by using this methodology when compared with those obtained numerically. An analytical solution using optimal HAM was obtained in Esmaeilpour and Ganji[7] and they concluded that this approach is more powerful and give results with higher accuracy when compared with other numerical techniques. The study[8] developed spectral HAM and compared the obtained numerical results with HAM. They came to a result, that spectral HAM converges at least twice as fast as HAM. HAM is also used in Moghimi et al.[9] to obtain the solution of convergent and divergent flows in the presence of magnetic field. The results were found to be comparable with those obtained numerically by using Fehlberg fourth-fifth order Runge-Kutta (RK) method. Like other mentioned studies, Sheikholeslami et al.[10] also preferred analytical approach of Adomian decomposition method (ADM) and found that it is a powerful technique and gives results with higher accuracy than numerical approach based on the RK method. They studied the effects of external uniform magnetic field and nano particles on flow in a convergent as well as in divergent channel. ADM as a powerful analytical approach was also used in Asadullah et al.[11] to obtain the solution of the problem and the results were compared with numerical results obtained by technique based on RK method. This work has significance in the sense that it involves the discussion of non-Newtonian fluid flow by considering Jeffery fluid model in a converging and diverging channel. The focus of the study[12] was to obtain analytical solution using ADM. The authors used Daun Rach Approach to obtain the solution of flow in a convergent and divergent channel. In order to see the geometrical effects on traditional Jeffery-Hamel flow,[13] extended such flows by considering stretchable convergent/divergent channel. They concluded that stretching results in dragging more fluid near walls for the case of convergent flow. They also highlighted that stretching causes the enhancement of heat transfer rate for convergent flow. Several industrial applications of non-Newtonian fluids appeal for their studies in different geometries and therefore, one can see that such studies have been made for the flows of non-Newtonian fluids between nonparallel walls such as those in Balmer and Kauzlaich,[14] Forsyth[15], Rajagopal et al.,[15] Chakraborty and Metzner,[17]7 Bhatnagar et al.,[18] and Baris.[19] Among them Balmer and Kauzlaich[14] discussed the flow in a convergent/divergent channel using power law fluid model. Whereas Forsyth[15] presented survey of some contemporary developments in converging polymer flow. Special attention was given to those theoretical and practical developments which explain flow discontinuities, and which can lead to simple predictive techniques. The flow of third grade non-Newtonian fluid was analyzed in detail[16] for converging/diverging types. The work[17] explained the fluid properties for non-Newtonian fluid by considering two-constant and three-parameter upper convected Maxwell-Oldroyd models. They concluded that the consideration of two-constant gives the same result except the quantitative differences.

The heat transport between nonparallel plane walls was actively addressed in addition to the discussion of the dynamics of fluids in these channels. There are three modalities of heat transfer but convection is the most applicable mode of heat transfer. Heat transfer is an important principle in biological systems and transportation of industrial and engineering fluids. The industrial applications include thermal insulation, surface catalysis of chemical reactions, cooling of nuclear reactors, microelectronic heat transfer equipment, thermal transport in petroleum industries, and thermal energy storage. The convective Jeffery-Hamel flow with heat transfer has received considerable attention due to its industrial applications especially for increasing efficiency of heat exchangers. In this context, the investigation[20] performed experimental study for converging and diverging tubes to determine the entry and fully developed region of heat transfer coefficients, pressure distribution, and friction factor at various taper angles. Whereas Garg and Maji[21] computationally showed that the technique of converging and diverging channel configuration can be used to achieve the enhancement of heat transfer. These channels can also be used in automobile gas-gas heat exchangers, radiators, and liquid-liquid plate heat exchangers among others. Such applications were explained in Yilmaz and Erdinc.[22,23] It is cited earlier that a number of studies were made on classical Jeffery-Hamel flow of Newtonian and Non-Newtonian fluids. In some cases, analytical solutions were obtained for the velocity profile while others computed numerical solutions. The literature survey on heat transfer analysis of Jeffery-Hamel flow shows that Millsaps and Pohlhausen[24] and Riley[25] obtained the exact solution of the energy equation. The heat transfer analysis of viscous fluid for Jeffery-Hamel flow was discussed by considering symmetry of the channel with no slip condition.[26] This work was extended in Khan et al.[27] for slip and temperature jump conditions. When coming to the analysis of thermal effects of such flows for Non-Newtonian fluids, a detailed analysis is made for second grade fluid in Hayat et al.[28,29] Applications of Jeffery-Hamel flows lead to the study of these flows for nano-fluids such as those in Rahimi Petroudi et al.,[30] Sheikholeslami et al.,[31] Dogonchi and Ganji,[32] and Mohyud-Din et al. [33] Among these Rahimi Petroudi et al.[30] applied collocation method for the solution of magneto-hydrodynamic Jeffery-Hamel flow of nano-fluids. They considered water as the base fluid. They concluded that the presence of nanoparticles in Newtonian fluid results into the reduction of velocity when Reynolds number is increased. Moreover, the back-flow disappears in case of convergent channel. The application of ADM to obtain analytical solution for the problem of nano-fluid flow can be viewed in Sheikholeslami et al.[31] Instead of simply applying ADM, DRA was used[32] to solve the problem of MHD radiating nano-fluid with water as base fluid lying between two nonparallel plane walls. The effects of stretching and shrinking of walls were also considered. The inclusion of these effects of stretching lead to the rise in velocity and temperature profiles. The effects of dynamic and thermal slips for nanofluid with water as the base fluid were explored in Mohyud-Din et al.[33] Analytical and numerical results were compared and found to be coincident. They concluded that backflow occurs near the walls for the case of divergent flow.

A closer look on the studies for instance[3–13] discloses that the transverse component of velocity is considered to be zero following.[34] This follows that flow was purely radial and transformed using similarity transformation by following the pioneering works, Jeffery[1] and Hamel.[2] In these works the flow is considered to be inertial which most of the time makes it difficult to find analytical solution of the problem. But there are investigations like Mansutti and Ramgopal[35] and Mansutti and Pontrelli[36] where non-inertial flows were addressed. In context of inertial flows, Rosenhead[37] found that the reversal of flow occurs and moreover there exists a bifurcating value of wedge angle beyond which in/out flows could not exist. Whereas such bifurcating value did not exist for noninertial flow as stated in Brewster et al.[38] The stability analysis for Jeffery-Hamel flow[39] was analyzed in detail and disclosed that IOI and IO flows are unstable for Reynolds number near zero.

Unlike the consideration of symmetric flow,[35] uniform slip along the wall[27,40] used more general boundary conditions called traction boundary conditions. The objective of the use of these boundary conditions was to analyze the impact of boundary stresses applied at the boundaries of the wedge. This results in the occurrence of slip and somewhere no-slip at the wall. They basically provided counter example to the comment made in Sochi[41] that slip is not a uniform phenomenon. Moreover, Harley et al.[40] did not use the condition of flow symmetry as was usually considered in Khan et al.[27] In this way, they basically desired to see the possible existence of asymmetric solution. For this purpose they introduced constant flow rate condition in the interval $[-\alpha, \alpha]$. Now we discuss the most recent literature[42–45] on Jeffery-Hamel flows. In these, Khan et al.[42] studied non-Newtonian fluid behavior by using Eyring-Powell model for Jeffery-Hamel flows. They used Haar wavelet approach to obtain numerical solution and compared the results with those obtained through fourth order RK method. The interesting thing in this study is that, a quite new numerical approach was adopted to solve the problem of Jeffery-Hamel flow. Another study[43] adopted new approach of differential transform method to solve the problem of Jeffery-Hamel flow. They studied the problem in the presence of gyrotactic microorganism and considered nanofluid for the analysis. They concluded that temperature and concentration profiles increase with increasing Brownian motion parameter for convergent as well as divergent flows. They also noticed that temperature profile decrease with an increase in Reynolds number. The study[44] focused on development of new solution methodology of Hemite wavelet method (HWM) to address the problem of Jeffery-Hamel flow. The authors made a detailed solution comparison with solutions obtained via differential transform method, homotopy perturbation method, variational iteration method, and RK method. Their results disclosed that HWM is more satisfactory than other used methodologies to solve the problem of Jeffery-Hamel flows. Another new approach of Taylor optimization method based on differential evolution algorithm for the solution of Jeffery-Hamel flows can be viewed in Ara et al.[45] But this study involves the discussion of non-Newtonian fluids by taking the micropolar fluid model. Finally, the numerical results were compared with those obtained through RK method for the sake of accuracy. The recent work[46] discussed the effects of boundary stresses on MHD flow of viscous fluids. They applied developed ADM based on DRA for nonlinear third order ordinary differential equations with mixed boundary conditions. They also used Gauss-Lobatto formula to for the discretization of boundary conditions to obtain numerical solution of the problem. The other interesting studies[47–57] can be consulted for thorough analysis on heat transfer in the presence of different important aspects of Soret/Dufour, mixed convection and radiation among others.

The detailed literature review discloses that no one has addressed the effects of Soret and Dufour along with viscous dissipation in the presence of boundary stresses. The purpose of present work is to model the problem of Jeffery Hamel flow in the presence of viscous dissipation and Soret/Dufour effects. The next objective is to adopt the approach of Harley et al.[40] and Asghar et al.[46] for the analysis of modeled problem. The problem is transformed using similarity transformation into coupled nonlinear ordinary differential equations. The above literature survey shows that different analytical and numerical approaches were adopted for the nonlinear coupled problems of Jeffery-Hamel flows. But none of the problem involve mixed boundary conditions for coupled problem. Therefore, the present study involves the numerical solution of such problem using the shooting method. The analysis is broken up into different sections in which formulation of the problem is presented in Section 2 whereas Section 3 is meant for the details of solution methodology. The main findings of the work are discussed in Section 4. Section 5 is dedicated for the conclusions drawn from the analysis.

Formulation of the problem

We consider an incompressible steady hydrodynamic flow of viscous fluid that lies between two walls inclined at an angle of 2α. The walls of the channel are maintained at constant temperatures and concentrations. The flow geometry is prescribed in the following Figure 1:

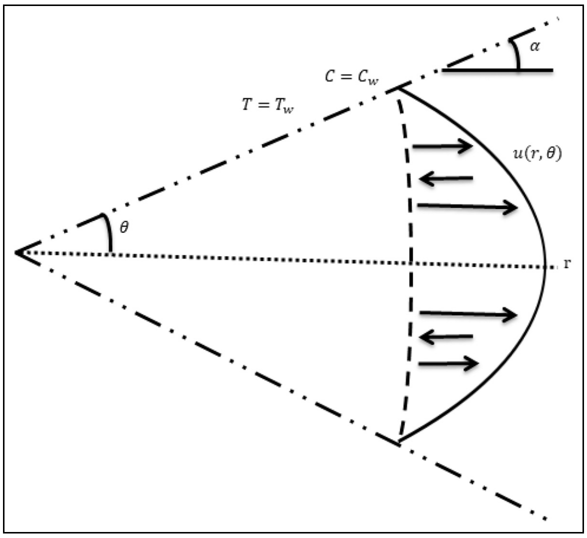

Figure 1. Geometry of the problem.

The equations governing the problem are,

$$0 = \frac{1}{r}\frac{\partial}{\partial r}(ru) + \frac{1}{r}\frac{\partial}{\partial \theta}(v(r,\theta)), \tag{1}$$

$$u\frac{\partial u}{\partial r} = -\frac{1}{\rho}\frac{\partial p}{\partial r} + v\left(\frac{\partial^2 u}{\partial r^2} + \frac{1}{r}\frac{\partial u}{\partial r} + \frac{1}{r^2}\frac{\partial^2 u}{\partial \theta^2} - \frac{u}{r^2}\right), \tag{2}$$

$$0 = \frac{1}{\rho r}\frac{\partial p}{\partial \theta} - \frac{2\nu}{r^2}\frac{\partial u}{\partial \theta}, \tag{3}$$

$$\begin{aligned}\rho c_p u\frac{\partial T}{\partial r} &= k\left[\frac{\partial^2 T}{\partial r^2} + \frac{1}{r}\frac{\partial T}{\partial r} + \frac{1}{r^2}\frac{\partial^2 T}{\partial \theta^2}\right] \\ &+ \mu\left[2\left(\left(\frac{\partial u}{\partial r}\right)^2 + \left(\frac{u}{r}\right)^2\right) + \frac{1}{r^2}\left(\frac{\partial u}{\partial \theta}\right)^2\right] \\ &+ \frac{DK_T}{C_s}\left[\frac{\partial^2 C}{\partial r^2} + \frac{1}{r}\frac{\partial C}{\partial r} + \frac{1}{r^2}\frac{\partial^2 C}{\partial \theta^2}\right],\end{aligned} \tag{4}$$

$$\begin{aligned}u\frac{\partial C}{\partial r} &= D\left[\frac{\partial^2 C}{\partial r^2} + \frac{1}{r}\frac{\partial C}{\partial r} + \frac{1}{r^2}\frac{\partial^2 C}{\partial \theta^2}\right] \\ &+ \frac{DK_T}{T_m}\left[\frac{\partial^2 T}{\partial r^2} + \frac{1}{r}\frac{\partial T}{\partial r} + \frac{1}{r^2}\frac{\partial^2 T}{\partial \theta^2}\right], 5\end{aligned} \tag{5}$$

where $u = u(r,\theta)$ is the radial component of velocity, $v = v(r,\theta)$ is the transverse component of velocity, ρ is the density of the fluid, $p = (r,\theta)$ is the pressure, ν is the kinematic viscosity, c_p is the specific heat, $T = T(r,\theta)$ is temperature, k is thermal conductivity, μ is dynamic viscosity, D is coefficient of mass diffusivity, K_T is thermal diffusion ratio, C_s is concentration susceptibility, $C = C(r,\theta)$ is concentration, and T_m is mean fluid temperature. We assume the unidirectional motion in radial direction, therefore, $v = 0$. Under this assumption the continuity equations yields,

$$f(\theta) = ru \ \text{orequivalently} u = f(\theta)/r. \tag{6}$$

On using the similarity transformations defined by

$$F(\eta) = \frac{f(\theta)}{U}, \ \beta(\eta) = \frac{r^2 T}{T_w}, \ \phi(\eta) = \frac{r^2 C}{C_w}, \ \eta = \frac{\theta}{\alpha}, \tag{7}$$

into equations (2)–(5) and eliminating the pressure gradient term from equations (2) and (3), we obtain a system of differential equations such as,

$$F'''(\eta) + 2\alpha \mathrm{Re} F(\eta)F'(\eta) + 4\alpha^2 F'(\eta) = 0, \tag{8}$$

$$\begin{aligned}&\beta''(\eta) + 2\alpha^2\left(2 + \frac{\Pr \mathrm{Re}}{\alpha}F(\eta)\right)\beta(\eta) \\ &+ \Pr Ec\left[4\alpha^2 F^2(\eta) + (F'(\eta))^2\right] \\ &+ D_f \Pr(\phi''(\eta) + 4\alpha^2\phi(\eta)) = 0,\end{aligned} \tag{9}$$

$$\begin{aligned}&\phi''(\eta) + 2\alpha^2\left(2 + \frac{\mathrm{Re} S_c}{\alpha}F(\eta)\right)\phi(\eta) \\ &+ S_c S_r(\beta''(\eta) + 4\alpha^2\beta(\eta)) = 0.\end{aligned} \tag{10}$$

Here $\mathrm{Re} = \frac{U\alpha}{\nu}$ is the Reynolds number, Pr is the Prandtl number, Ec is the Eckert number, D_f is the Dufour number, S_c is the Schmidt number, S_r is the Soret number. These dimensionless numbers are defined by,

$$\Pr = \frac{\mu c_p}{k}, Ec = \frac{U^2}{c_p T_w}, D_f = \frac{D K_T C_w}{\nu c_p C_s T_w},$$
$$S_c = \frac{\nu}{D}, S_r = \frac{D K_T T_w}{\nu T_m C_w}.$$

The channel is said to be divergent for $\alpha > 0$ and $U > 0$ whereas it is convergent when $\alpha < 0$ and $U < 0$. The aim of present work is to analyze the impact of boundary stresses that are applied at the boundaries of the wedge. These boundary stresses are defined through traction boundary conditions which highlight the non-uniformity of slip. The simplified form of momentum equations, equation (8), is solved over the whole domain $[-\alpha, \alpha]$ so that an analysis can be made for the stresses applied at both walls of the wedge. For the uniqueness of velocity, we need one more condition. This condition is specified as volume flow rate condition and is given by

$$q = \int_{-1}^{1} F(\eta) d\eta. \tag{11}$$

In this way we do not constrain the symmetry of the channel. The Cauchy stress tensor for viscous fluids is defined as

$$\mathbf{T} = -p\mathbf{I} + \mu\left((\nabla\mathbf{V}) + (\nabla\mathbf{V})^t\right), \tag{12}$$

where $\mathbf{V} = [u(r,\theta), 0, 0]$ and $\nabla = \left[\frac{\partial}{\partial r}, \frac{1}{r}\frac{\partial}{\partial \theta}, \frac{\partial}{\partial z}\right]$. The form of stress tensor on invoking equations (3) and (4) becomes,

$$\mathbf{T} = \begin{pmatrix} -p - \frac{2\alpha F(\eta)}{r^2} & \frac{F'(\eta)}{r^2} & 0 \\ \frac{F'(\eta)}{r^2} & -p + \frac{2\alpha F(\eta)}{r^2} & 0 \\ 0 & 0 & -p \end{pmatrix}. \tag{13}$$

Now we move toward the construction of traction boundary condition which is defined by $\mathbf{t} = \mathbf{T} \cdot \mathbf{n}$, where $\mathbf{n}$ is the unit vector normal to the surface. The unit vectors normal to the surface are defined by

$$n_r = (\cos\theta, \sin\theta, 0),\ n_\theta = (-\sin\theta, \cos\theta, 0),$$
$$n_z = (0, 0, 1). \tag{14}$$

Finally, the traction boundary conditions get the form,

$$\mathbf{t}_r = -p\cos\theta + \frac{-2\alpha(\cos\theta)F(\eta) + (\sin\theta)F'(\eta)}{\tilde{r}^2},$$
$$\mathbf{t}_\theta = -p\sin\theta + \frac{2\alpha F(\eta)(\sin\theta) + (\cos\theta)F'(\eta)}{\tilde{r}^2},\ \mathbf{t}_z = 0, 15 \tag{15}$$

where $\tilde{r}$ is a specified value of r. Now in order to have numerically employable boundary conditions that are representative of the traction condition at the boundary of the wedge let us set $\theta-$ component of equation (15) as zero. Therefore, it yields

$$p(\tilde{r}, \theta) = \frac{2\alpha F(\eta) + (\cot\theta)F'(\eta)}{\tilde{r}^2}. \tag{16}$$

Invoking this expression into $\mathbf{t}_r$ leads to the following,

$$tr = -\frac{\csc\theta(2\alpha F(\eta)\sin(2\theta) + (\cos(2\theta))F'(\eta))}{r^2}. \tag{17}$$

Since this condition is valid along the boundaries, therefore we apply it at $\theta = \pm\alpha$ or in other words at $\eta = \pm 1$. This results into,

$$tr = -\frac{\csc(\pm\alpha)(2F(\pm 1)\alpha\sin(\pm 2\alpha) + \cos(\pm 2\alpha)F'(\pm 1))}{2\tilde{r}^2}. \tag{18}$$

The rest of the boundary conditions for temperature and concentration are

$$T = \frac{T_w}{r^2},\ \ , C = \frac{C_w}{r^2},\ \ \text{at}\theta = \pm\alpha.$$

Which in the light of quantities introduced in equation (7), become

$$\beta = 1,\ \ \phi = 1,\ \ \text{at}\eta = \pm 1. \tag{19}$$

Solution of the problem

The governing equations, equations (8)–(10) are coupled nonlinear system of equations. We have to solve them subject to constant flow rate condition given in equation (11), mixed boundary conditions defined in equation (18) and Dirichlet conditions prescribed in equation (19). The numerical shooting method is adopted as an iterative scheme to solve this problem. In this method, the system of differential equations are converted into a system of first order initial value problems. Then this system is solved by forward marching from $\eta = -1$ to $\eta = 1$ using Range-Kutta method of order 4 with the help of initial conditions given below in flow chart of the methodology. The initial guess u_i for $i = 1, 2, \cdots, 5$ are chosen in such a way that the following conditions are satisfied at $\eta = \pm 1$

$$tr + \frac{\csc(-\alpha)(2y_1(-1)\alpha\sin(-2\alpha) + \cos(-2\alpha)y_2(-1))}{2\tilde{r}^2} = 0,$$
$$tr + \frac{\csc(+\alpha)(2y_1(+1)\alpha\sin(+2\alpha) + \cos(+2\alpha)y_2(+1))}{2\tilde{r}^2} = 0,$$
$$\int_{-1}^{1} y_1 d\eta - q = 0,$$
$$y_4(1) - 1 = 0,$$
$$y_6(1) - 1 = 0.$$

Where $y_1 = F, y_2 = F', y_3 = F'', y_4 = \beta, y_5 = \beta'$, $y_6 = \phi, y_7 = \phi'$. To choose u_i, first of all we choose some arbitrary values and then apply Newton's method to iterate the process until the required values of u_i are obtained. A similar procedure is adopted to achieve the required results for other parameters. The numerical results are compared for accuracy with analytical results[46] obtained by Adomian decomposition method using Daun Rach Approach. The results are in great agreement and are presented in Table 1. The method is described in the following flow chart:

Table 1. Validation of numerical and analytical results.

η	Present results for F(η)%	Results of Asghar et al.[46] F(η)%	Absolute error|[46] −Present results|
−1.0	0.004139	0.004058	0.000081
−0.8	0.133604	0.133509	0.000095
−0.6	0.237799	0.237632	0.000167
−0.4	0.314646	0.314489	0.000157
−0.2	0.361892	0.361719	0.000173
0.0	0.377848	0.377671	0.000177
0.2	0.361892	0.361719	0.000173
0.4	0.314646	0.314489	0.000157
0.6	0.237799	0.237632	0.000167
0.8	0.133604	0.133509	0.000095
1.0	0.004139	0.004058	0.000081

Results and discussion

We have mathematically modeled the problem of Jeffery-Hamel flow in the presence viscous dissipation, thermo-diffusion, and diffusion-thermo effects. The traction boundary conditions that represent the

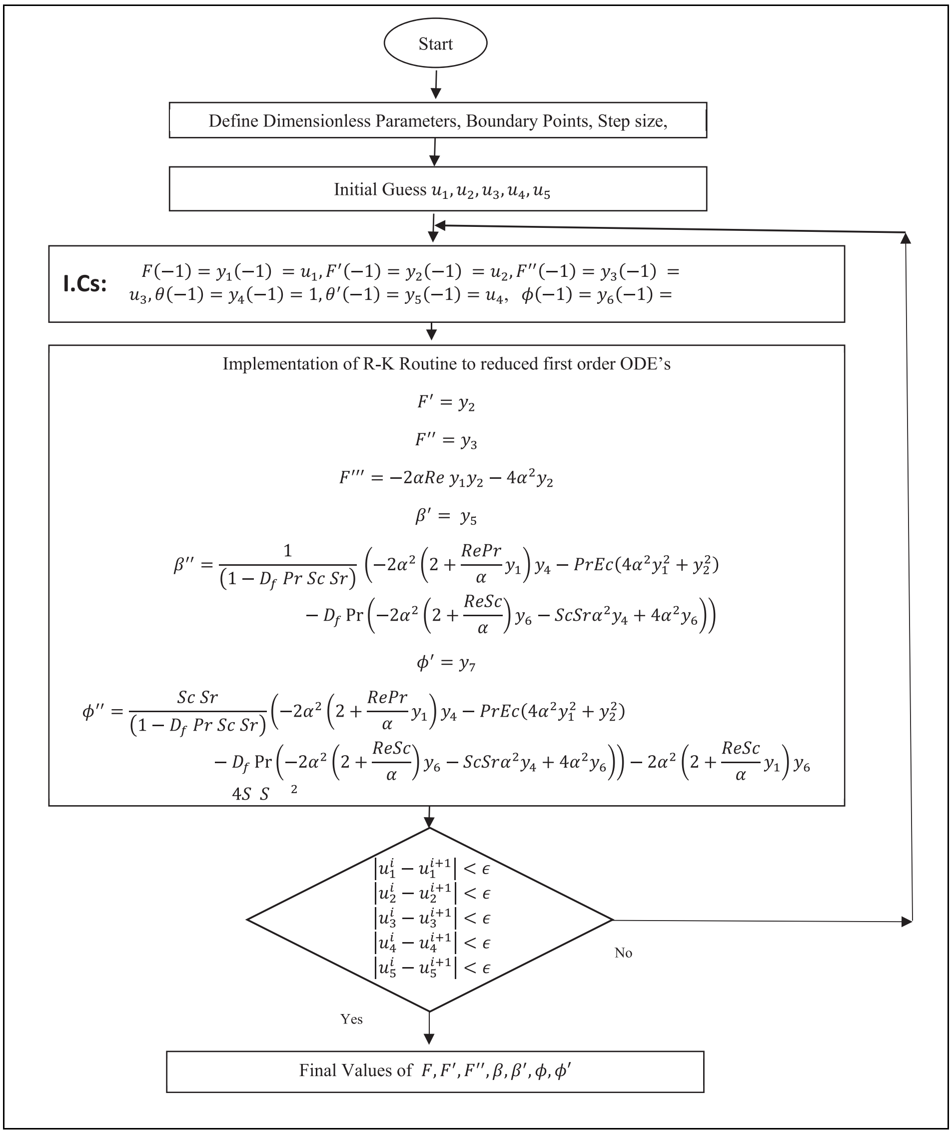

boundary stresses are also modeled and found as mixed type of boundary conditions. The shooting method is developed to accommodate such boundary conditions for nonlinear system of coupled ordinary differential equations. Then the problem is solved numerically using shooting method. In order to check the accuracy of numerical results by shooting scheme, they are compared with those presented in Asghar et al.[46] and found completely agreeing with each other. This comparison is presented in Table 1. This section is meant to throw light on the effects of apposite parameters comprising of angle between nonparallel walls (α), Reynolds number (Re) to describe inertial effects, traction parameter (tr) to address boundary stresses, on velocity, temperature, and concentration profiles. Whereas the effects of other important parameters such as Dufour number $\left(D_f\right)$, Soret number (Sr), Prandtl number (Pr), Eckert number (Ec), and Schmidt number (Sc) on temperature and concentration profiles are portrayed graphically. There are two other important features of present study, one of which is that it is free from assumption of symmetry of the channel which most of the time is considered for the analysis of Jeffery-Hamel flow in a convergent/divergent channels, see Esmaeilpour and Ganji,[7] Motsa et al.,[8] Moghimi et al.,[9] and Sheikholeslami et al.[10] The other feature is that it does not involve the assumption of uniform slip by following Harley et al.[40] The graphical discussion of numerical results is divided into subsections, namely, velocity profile and temperature and concentration profiles:

Velocity profile

This subsection describes the effects of governing parameters, angle between nonparallel lines (α), Reynolds number (Re), and traction (tr) on velocity profile. The effects of these parameters are displayed in Figures 2 to 5. Figure 2 is constructed to see possible flow behaviors observed for inertial and non-inertial flows in a convergent or divergent channels. This figure highlights the existence of flow asymmetry that is captured and presented in Figure 2(b). The symmetric nature is also captured which can be seen in Figure 2(a). The flow reversal is captured and can be viewed both in Figure 2(a) and (b). The slip is also captured and shown in Figure 2. The variety of flow behaviors is caused due to the consideration of boundary stresses, flow free from assumption of symmetry and the problem in entire domain $[-\alpha, \alpha]$. In this way, one can infer that flow symmetry is not a uniform phenomenon but merely could be an assumption. Therefore, the use of such boundary conditions will help to improve the physical analysis of studies like[3–14] and many other investigations on flow in a convergent/divergent channels. Figure 3 is to see the velocity profile in non-inertial case with the variation of wedge angle. It is noticed that flow reversal occurs for the case of divergent/convergent flows. The case of IOI flow is observed for divergent flow for chosen values of parameters and this case is classified as unstable in[39] for the case of low Reynolds number. Although one can check the stability of the present problem for the classification based on stability. The flow behavior is OIO for the case of convergent flow. It is also seen that the flow regime is switched throughout the channel when one moves from the divergent to the case of convergent flow. Here we see that no-slip occurs only for divergent flow. Whereas slip is observed for both the cases of convergent and divergent flows. This figure shows that slip is not a uniform phenomenon. From literature review we come to know that[41] made a comment

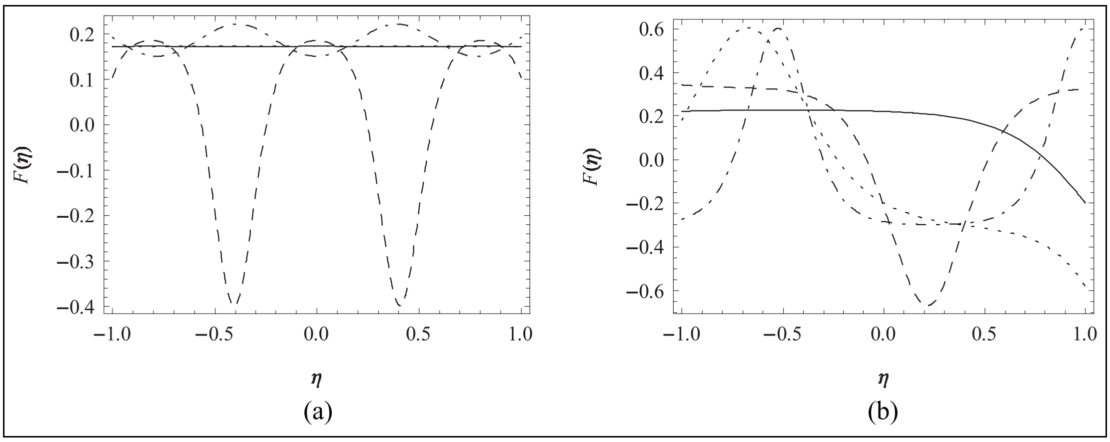

Figure 2. Possible behavior of velocity profile.

Fig.2(a)—$Re = 2000, r = 2, \alpha = 5^\circ, tr = 0$, ...$Re = 500, r = 2, \alpha = -5^\circ, tr = 0$
—$Re = 2000, r = 0.9, \alpha = -15^\circ, tr = -2.5$, $-\cdot-\cdot$ $Re = 2000, r = 0.9, \alpha = 5^\circ, tr = -2$
Fig.2(b)—$Re = 500, r = 2, \alpha = -5^\circ, tr = -2.5$, ...$Re = 500, r = 2, \alpha = 5^\circ, tr = 2.5$
—$Re = 1000, r = 0.5, \alpha = -5^\circ, tr = 2$, $-\cdot-\cdot$ $Re = 2000, r = 0.9, \alpha = 5^\circ, tr = 2$

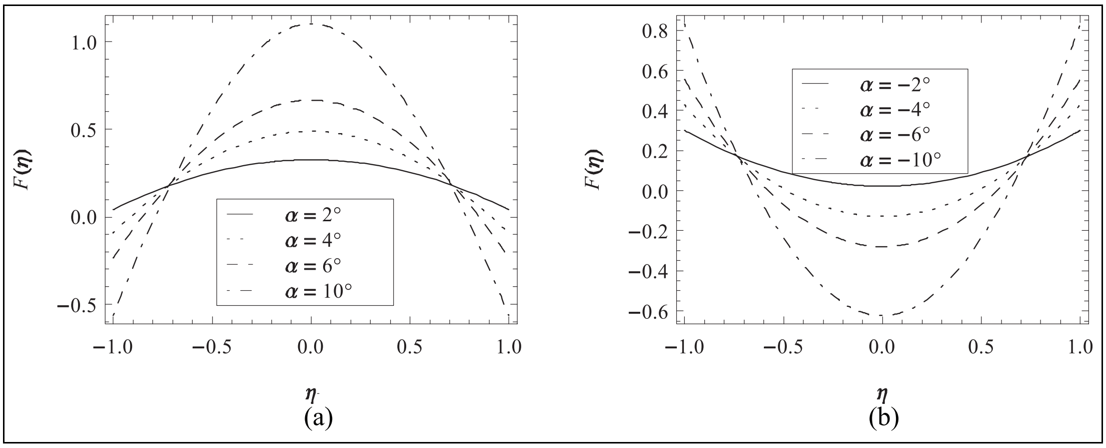

Figure 3. Velocity profile for $\tilde{r} = 2$, Re = 10, $tr = 2$, $q = 0.5$.

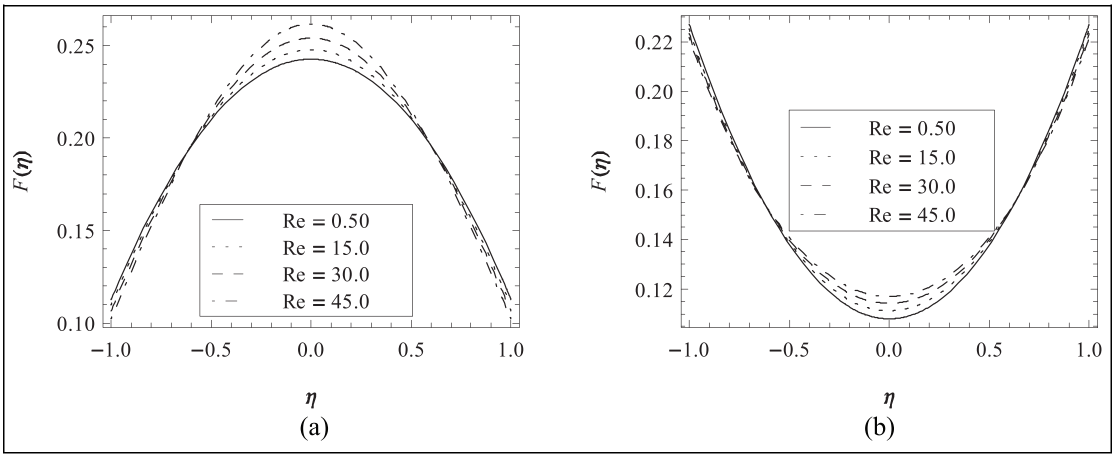

Figure 4. Velocity profile for $\tilde{r} = 2$, $tr = 0.25$, $q = 0.5$ with (a) $\alpha = 7^{\circ}$ (b) $\alpha = -7^{\circ}$.

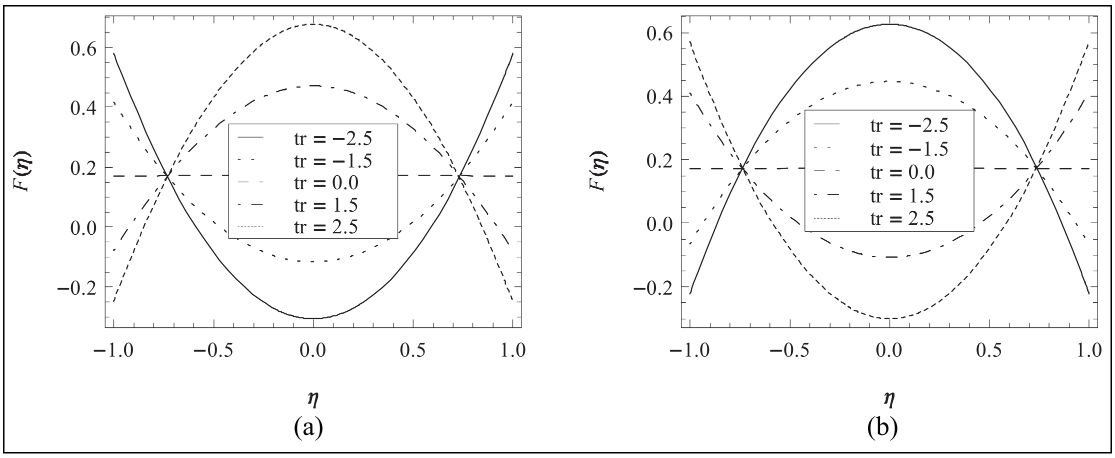

Figure 5. Velocity profile for $\tilde{r} = 2$, $Re = 10$, $q = 0.5$ with(a) $\alpha = 5^{\circ}$ (b) $\alpha = -5^{\circ}$.

in his experimental work that slip is not a uniform phenomenon. Therefore, we can say that Figure 3 is a counter example for Sochi.[41] Therefore, it suggests that instead of using no-slip (uniform) condition for flow through venturi meter[58,59] and convergent-divergent nozzle,[60] one must take traction boundary conditions. As, it will definitely help to explore the design properties of venturi tubes and convergent-divergent nozzles and will bring improvement in design. The traction boundary conditions can also be

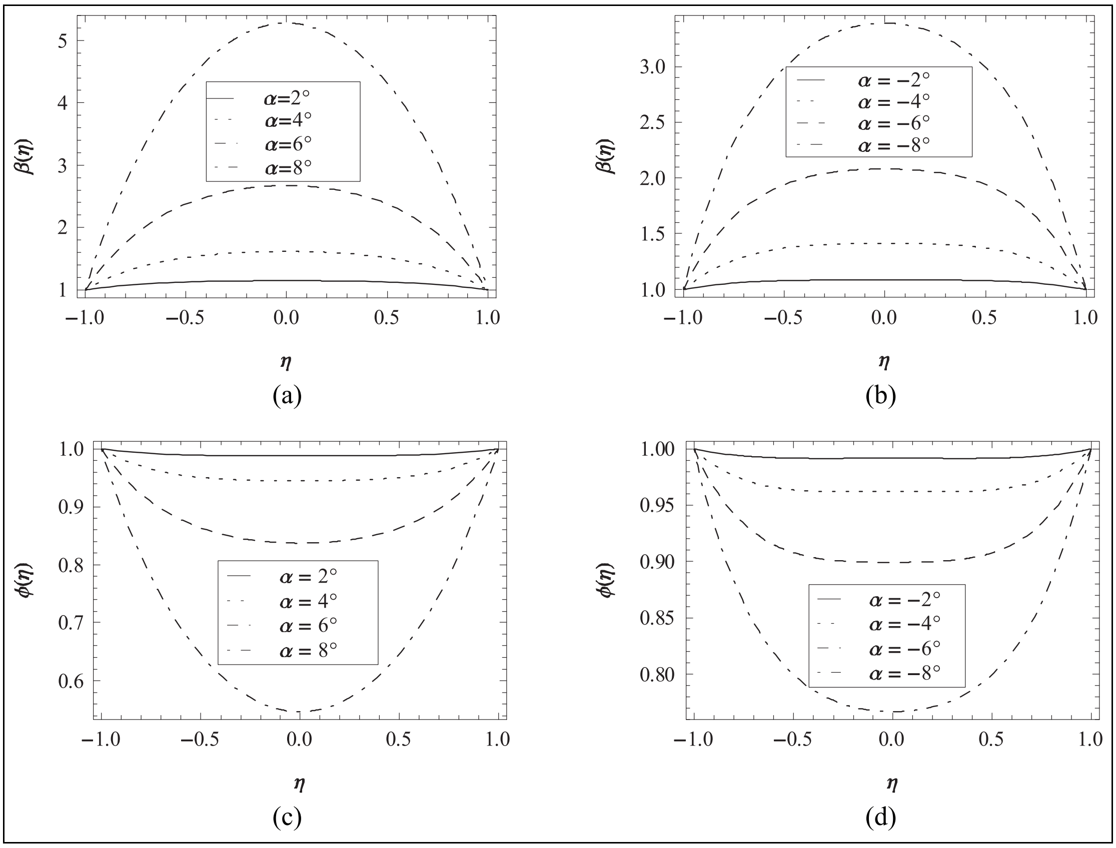

Figure 6. Temperature and concentration profiles for $\tilde{r} = 2$, $Re = 0.5$, $tr = 2$, $q = 0.5$, $Ec = 0.3$, $D_f = 0.5$, $Pr = 7.0$, $Sc = 0.62$, $Sr = 0.2$.

invoked for the flow through Tesla valve,[61] where no-slip conditions were assumed. It can be hoped that this consideration can help to optimize the angle. In Figures 4 and 5, the left panels are for divergent flow however, the right panels are for convergent flow. Figure 4 highlights the effects of Reynolds number while keeping the values of other parameters fixed. It is observed that slip occurs both for convergent and divergent flows. The outflow as well as nonuniform slip are also captured. The behavior of velocity profile with the variation of most pertinent parameter of the problem (tr) are shown in Figure 5. It is interesting to see that the boundary layer is observed for the case of non-zero values of traction parameter and the boundary layer disappears for zero value of traction parameter. Increasing values of traction parameter both for $tr \in \mathbb{R}^+$ and $tr \in \mathbb{R}^-$ pop ups the boundary layer. It is noticed that flow behavior becomes opposite while moving from divergent to convergent flow consideration. This property also leads to the fact that no-slip needs not to be recovered in the absence of boundary stresses ($tr = 0$).

Temperature and concentration profiles

The influence of different thermo-physical parameters on the temperature and concentration profiles are illustrated in Figures 6 to 14. The left panels for each of these figures are for the divergent flow whereas, the right panels are for convergent flows. Since we considered the problem of Newtonian fluid, therefore, Schmidt number (Sc) is chosen for hydrogen ($Sc = 0.22$), water vapor ($Sc = 0.62$) and ammonia ($Sc = 0.78$) at $25^{\circ}C$. Whereas, at the same temperature of 25°C, the Prandtl number is taken to be $\Pr = 0.7, 2.36, 7$, for air, carbon disulfide and water respectively. Figure 6 shows that temperature profile is mostly parabolic in nature and is concave down which means that extreme values occur at center and near walls of the channel. The thermal boundary layer strengthens by expanding the channel. The thermal boundary layer is more pronounced for divergent flow when compared with convergent flow profile. The Figure 6(c) and (d) are to highlight the effects of increase in angle between non-parallel walls on concentration profile. The behavior is quite opposite to what is observed in case of temperature profile. Figure 7 reflects inertial effects on the temperature and concentration profiles. The thermal and concentration boundary layers strengthen with the strength of inertial effects. Here it is important to mention that we have made this comparison for water ($Pr = 7.0$). The boundary layer effects also fortify for divergent flow. The influence of one of the leading parameter

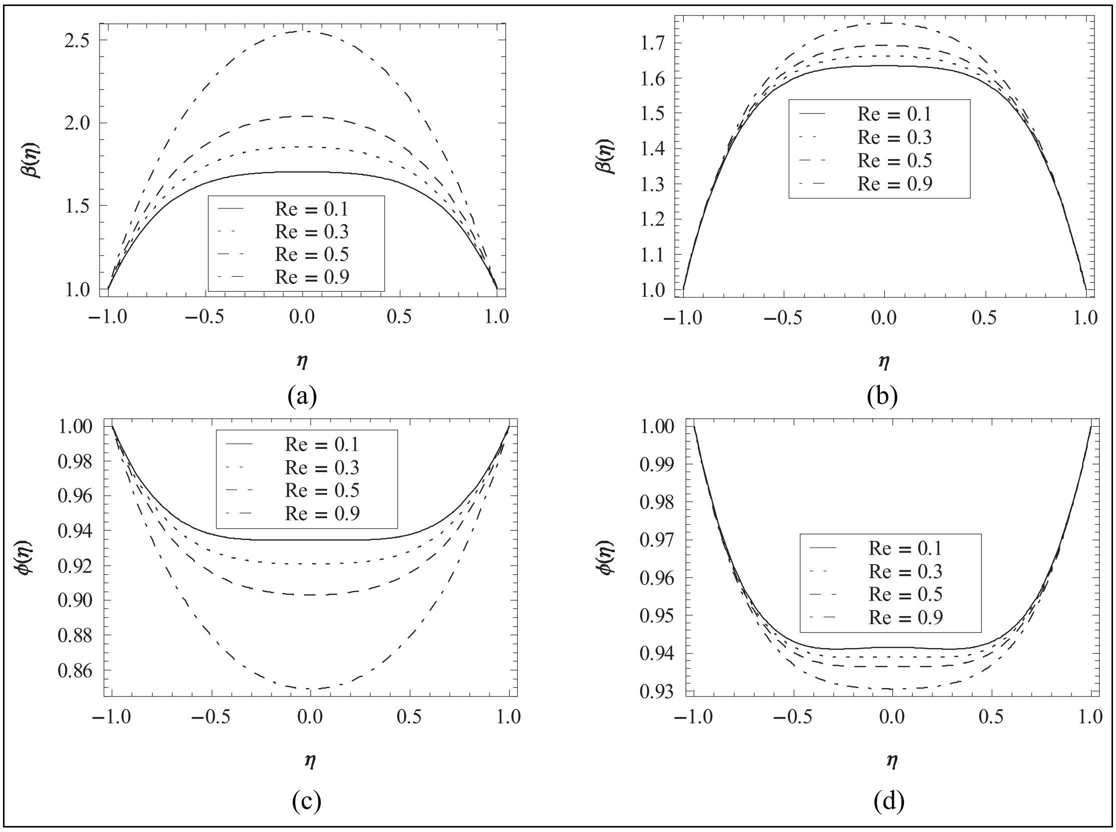

Figure 7. Temperature and concentration profiles for $\tilde{r} = 2, tr = 2, q = 0.5, Ec = 0.3, D_f = 0.5$, Pr $= 7.0, Sc = 0.62, Sr = 0.2, \alpha = |5°|$.

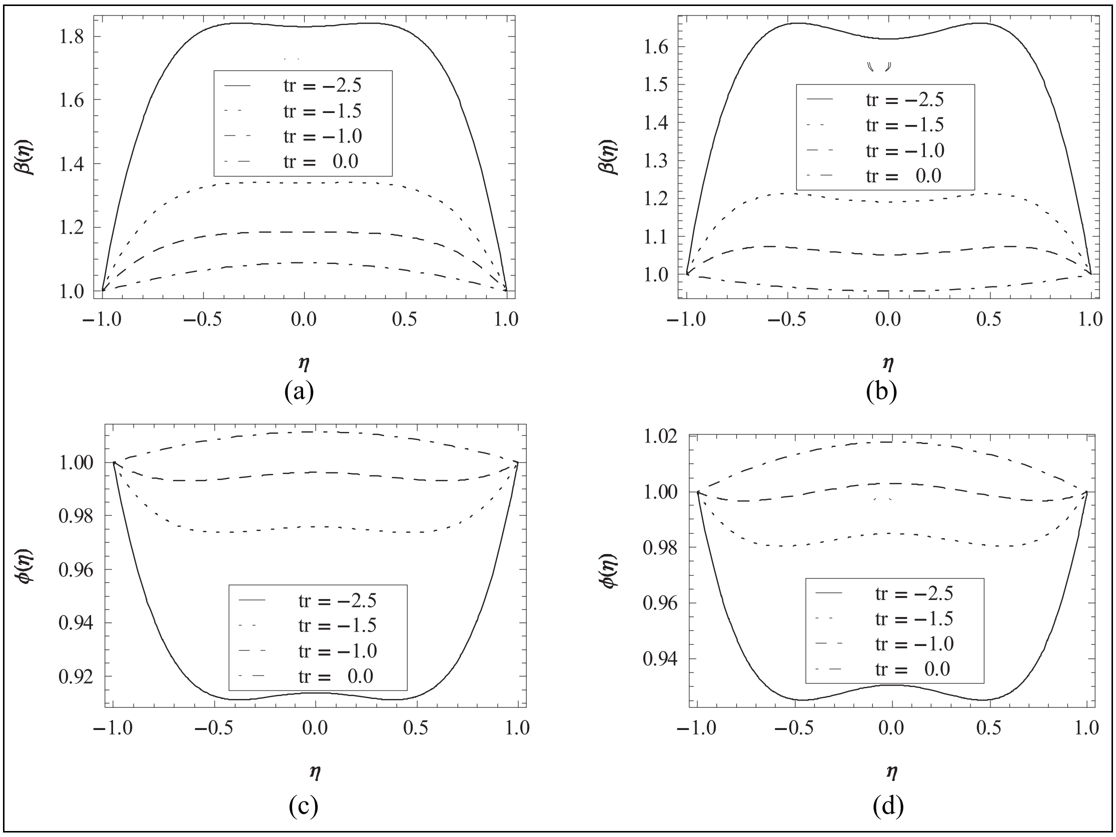

Figure 8. Temperature and concentration profiles for $\tilde{r} = 2$, Re $= 0.5, q = 0.5, Ec = 0.3, D_f = 0.5$, Pr $= 7.0, Sc = 0.62, Sr = 0.2, \alpha = |5°|$.

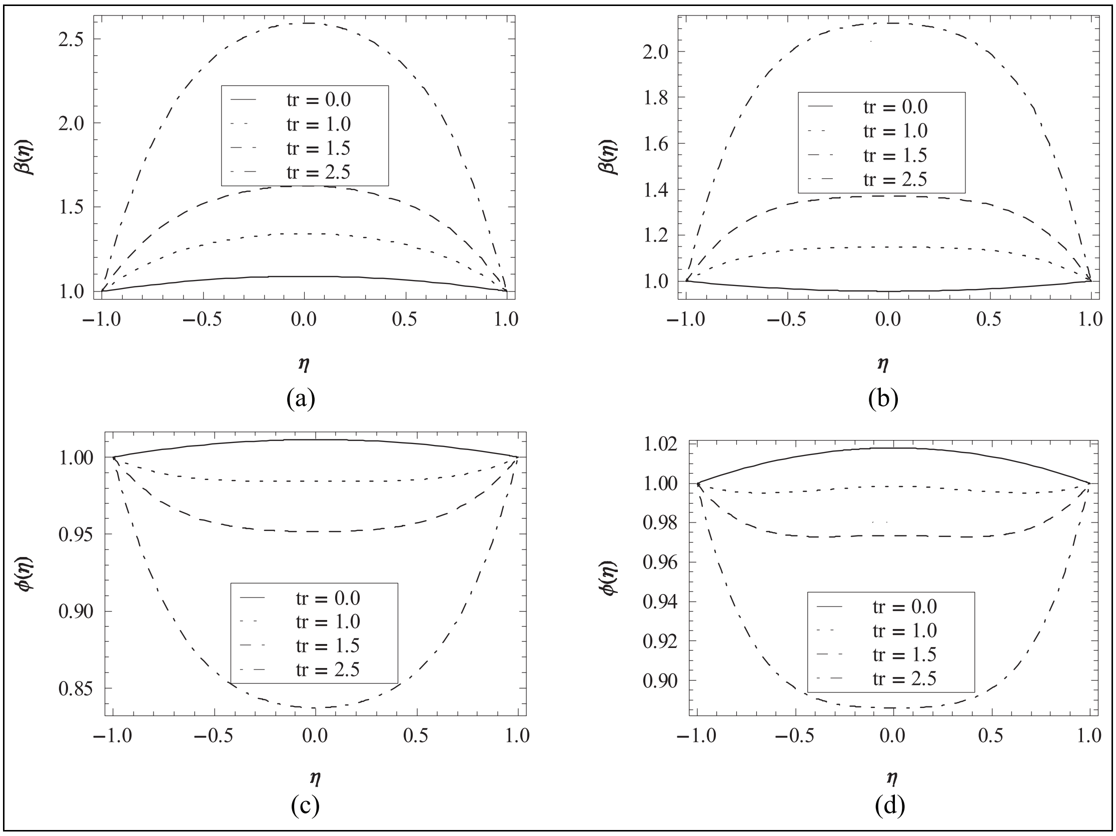

Figure 9. Temperature and concentration profiles for $\widetilde{r} = 2$, Re = 0.5, $q = 0.5$, $Ec = 0.3$, $D_f = 0.5$, Pr = 7.0, $Sc = 0.62$, $Sr = 0.2$, $\alpha = |5°|$.

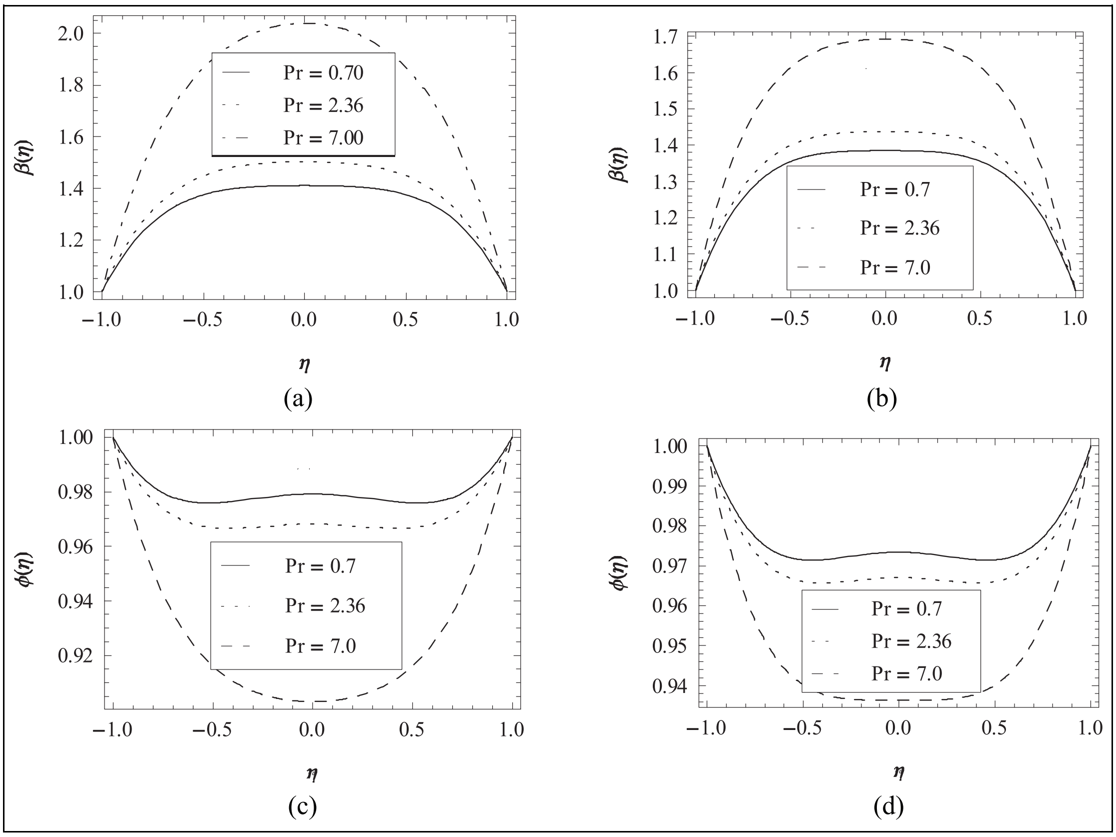

Figure 10. Temperature and concentration profiles with $tr = 2$, Re = 0.5, $q = 0.5$, $Ec = 0.3$, $\widetilde{r} = 2$, $D_f = 0.5$, $Sc = 0.62$, $Sr = 0.2$, $\alpha = |5°|$.

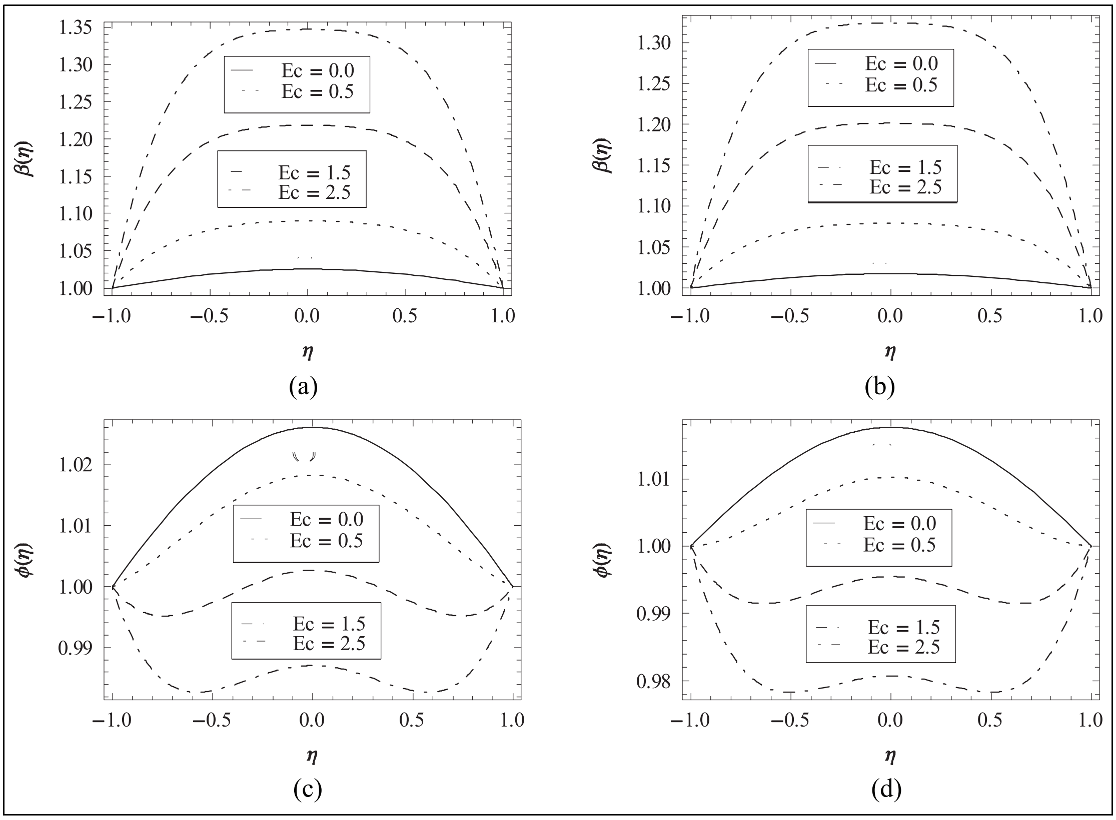

Figure 11. Temperature and concentration profiles with $tr = 2$, $\mathrm{Re} = 0.5$, $q = 0.5$, $\mathrm{Pr} = 0.7$, $\tilde{r} = 2$, $D_f = 0.5$, $Sc = 0.62$, $Sr = 0.2$, $\alpha = |5°|$.

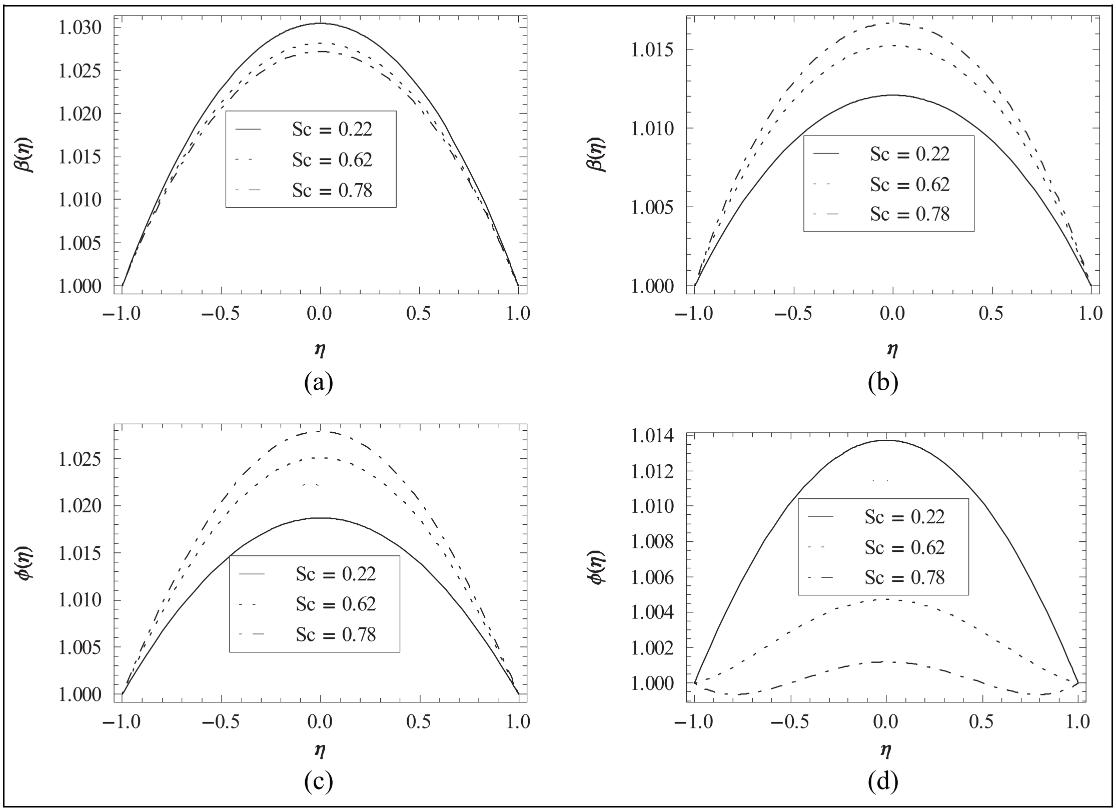

Figure 12. Temperature and concentration profiles with $tr = 0.5$, $\mathrm{Re} = 0.9$, $q = 0.5$, $\mathrm{Pr} = 0.7$, $\tilde{r} = 2$, $D_f = 0.5$, $Ec = 0.3$, $Sr = 0.3$, $\alpha = |5°|$.

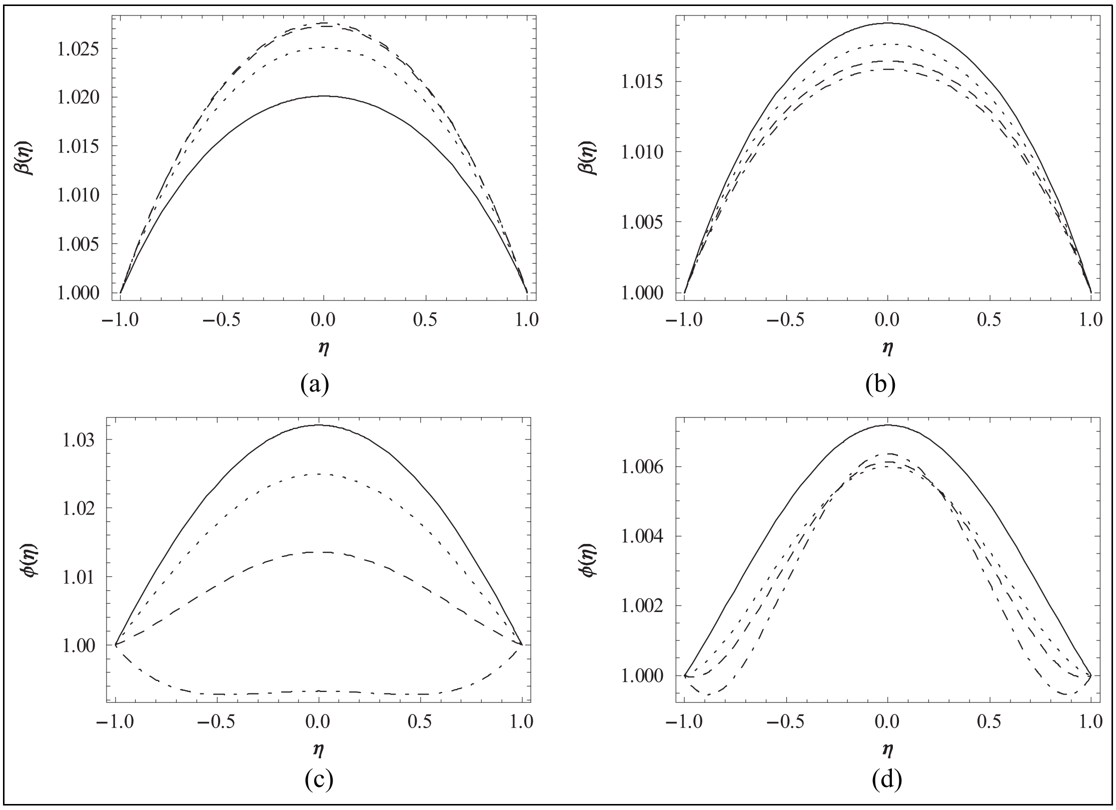

Figure 13. Temperature and concentration profiles with $tr = 0.5$, $\mathrm{Re} = 0.5$, $q = 0.5$, $\mathrm{Pr} = 0.7$, $\tilde{r} = 2$, $Ec = 0.5$, $\alpha = |5°|$, $Sc = 1.6$., — $Sr = 0.2$, $D_f = 0.6$, $\cdots$ $Sr = 0.5$, $D_f = 0.3$, — — $Sr = 1.0$, $D_f = 0.12$, — · — · $Sr = 2.0$, $D_f = 0.03$.

representing boundary stresses (tr) on temperature and concentration profiles is presented in Figure 8. The boundary layers are strongly affected by the presence of boundary stresses. It is observed that it affects the concavity of temperature and concentration profiles. Therefore, optimum values of temperature and concentration profiles change by changing traction parameter. Here we observe from Figure 8(a) that the presence of boundary stresses ($tr = -1, -1.5, -2.5$) at $\eta = 0$ quantitatively results an increase of 9.62%, 25.18%, and 74.16% in temperature when compared with temperature in the absence of boundary stresses, $tr = 0$. Therefore, the consideration of boundary stresses leave greater impact on temperature profile for coupled problem of Jeffery-Hamel flow. If we visit the concentration profile, Figure 8(c) for divergent flow, we see that the presence of boundary stresses ($tr = -1, -1.5, -2.5$) at $\eta = 0$ causes 1.5%, 3.5% and 9.74% increase in concentration. This increase is also significant but weaker in comparison to the temperature profile. The case of convergent flow Figure 8(b) and (d) shows that the presence of boundary stresses leave the same effect as discussed for divergent case. The effects of positive values of traction parameter are shown in Figure 9. The temperature and concentration profiles again show that the presence of boundary stresses affects greatly the respective boundary layers. The temperature profile is parabolic, therefore, the optimum values occur at the center and near the walls. It is also observed that thermal and concentration boundary layers weaken in the absence of boundary stresses ($tr = 0$). Figure 10 shows the effects of Prandtl number on temperature and concentration. Generally, the chosen values of Prandtl number are considered for characterization of liquids and gases. Here we observe that the optimum value of temperature is higher for liquids than for gases. This can be seen in Figure 10(a). Figure 10(b) shows that temperature profile behaves like the case of divergent flow. The difference is only of rate of increase of temperature. The behavior of concentration profile is depicted in Figure 10(c) and (d). The behavior is quite opposite to what was observed for temperature. Here we note that for smaller values of Pr, the thermal boundary layer weakens when compared to the effects of larger values of Pr. It is observed that increasing Pr results in increase of temperature and Khan et al[42] captured the same behavior. Whereas concentration decreases with increasing values of Pr. This is due to the fact that momentum boundary layer reinforces when compared to the thermal boundary layer. The impact of Eckert number (Ec) on temperature and concentration is highlighted in Figure 11(a) to (d). The larger the Ec, the greater the phenomenon of self heating. Therefore, we notice that temperature increases by increasing Ec which was also observed in Khan et al.[42] However, the concentration decreases with the increasing variation of Ec. The influence of Schmidt number (Sc) on temperature and concentration profiles are displayed in Figure 12. The values of

Sc are considered as $Sc = 0.22, 0.62, 0.78$ for hydrogen, water vapor, and ammonia respectively at 25 °C. It is observed that temperature increases, however, concentration profile decays by increasing Sc. Physically, the increase of Sc means a decrease of molecular diffusion. Therefore, the species concentration is higher for large values of Sc but lower for small values of Sc. Figure 13 shows the influence of Soret (Sr) and Dufour (D_f) numbers on temperature and concentration profiles while fixing other parameters. These profiles are quite opposite for convergent and divergent flows. We note that temperature increases by increasing Sr and decreasing D_f for divergent flow, however, concentration decreases with such variations. Similar observations were captured in Tsai and Huang[56] and Makinde and Olanrewaju.[57] Unlike other cases, here we notice the coupled effects in the profiles of concentration for convergent flow which may be due to introduction of boundary stresses and they were not captured in Tsai and Huang[56] and Makinde and Olanrewaju.[57]

Conclusions

We have mathematically modeled the problem of Jeffery-Hamel flow in the presence viscous dissipation, thermo-diffusion and diffusion-thermo effects. The problem is solved using shooting method and the results are compared with Asghar et al.[46] and found comparable. The purpose of present work is to study the influence of boundary stresses on convective Jeffery-Hamel flow of Newtonian fluid. We have made the following main findings from the detailed discussion of the problem under consideration:

- Slip is not a uniform phenomenon for the Jeffery-Hamel flow in a convergent/divergent channel which can be highlighted due to presence of boundary stresses and the same, also captured in Figures 2 and 3.
- Flow asymmetry can be captured due to presence of boundary stresses and by considering the flow in whole domain of $[-\alpha, \alpha]$
- Figure 3 shows that reversal of flow occurs for the cases of Jeffery-Hamel flows in the presence of boundary stresses.
- Here we observe IOI and OIO behaviors for divergent and convergent flows respectively, see Figure 3. It is concluded that bifurcations in flow occur.
- Figures 5 and 8 suggest that consideration of boundary stresses is important for Jeffery Hamel flows because boundary layers are majorly affected by such consideration.
- Boundary layer completely disappears in the absence of boundary stresses ($tr = 0$) which is observed in Figure 5.
- Outflows and Inflows are more pronounced by strengthening boundary stresses, see Figure 5.
- The effects of coupling are observed for velocity profile both for convergent and divergent flows as is observed in Figure 5.
- Figure 8(a) reveals that the presence of boundary stresses for $tr = -1, -1.5, -2.5$ at $\eta = 0$, causes the occurrence of an increase of 9.62%, 25.18%, 74.16% in temperature for divergent flow.
- Figure 8(c) reveals that the presence of boundary stresses for $tr = -1, -1.5, -2.5$ at $\eta = 0$, causes the occurrence of an increase of 1.5%, 3.5%, 9.74% in concentration for divergent flow.
- It can be viewed in Figure 10 that the optimum temperature is higher for liquids than for gases. The behavior of concentration is opposite when compared to the temperature.
- Figure 11 reflects that temperature increases whereas concentration decreases by increasing Eckert number (Ec). This result is due to self heating.
- Figure 12 shows that temperature increases but concentration decreases with decrease of molecular diffusion, that is, by increasing Sc.
- It is concluded from Figure 13 that temperature increases by increasing Sr and decreasing D_f for divergent flow, however, concentration decreases with such variations of Sr and D_f.

Declaration of conflicting interests

The author(s) declared no potential conflicts of interest with respect to the research, authorship, and/or publication of this article.

Funding

The author(s) received no financial support for the research, authorship, and/or publication of this article.

References

1. Jeffery GB. L. The two-dimensional steady motion of a viscous fluid. *Lond Edinb* 1915; 29: 455–465.
2. Hamel G. Spiralformige Bewgungen Zaher Flussigkeiten. *Jahresberricht der Deutschen Math Vereinigung* 1917; 25: 34–60.
3. Rosenhead L. The steady two-dimensional radial flow of viscous fluid between two inclined plane walls. *Proc Royal Soc A* 1940; 175: 436–467.
4. Makinde OD and Mhone PY. Hermite–Padé approximation approach to MHD Jeffery–Hamel flows. *Appl Math Comput* 2006; 181: 966–972.
5. Esmaili Q, Ramiar A, Alizadeh E, et al. An approximation of the analytical solution of the Jeffery–Hamel flow by decomposition method. *Phys Lett A* 2008; 372: 3434–3439.
6. Domairry DG, Mohsenzadeh A and Famouri M. The application of homotopy analysis method to solve nonlinear differential equation governing Jeffery–Hamel flow. *Commun Nonlinear Sci Numer Simul* 2009; 14: 85–95.

7. Esmaeilpour M and Ganji DD. Solution of the Jeffery–Hamel flow problem by optimal homotopy asymptotic method. *Comput Math Appl* 2010; 59: 3405–3411.
8. Motsa SS, Sibanda P, Awad FG, et al. A new spectral-homotopy analysis method for the MHD Jeffery–Hamel problem. *Comput Fluids* 2010; 39: 1219–1225.
9. Moghimi SM, Domairry G, Soleimani S, et al. Application of homotopy analysis method to solve MHD Jeffery–Hamel flows in non-parallel walls. *Adv Eng Softw* 2011; 42: 108–113.
10. Sheikholeslami M, Ganji DD, Ashorynejad HR, et al. Analytical investigation of Jeffery-Hamel flow with high magnetic field and nanoparticle by Adomian decomposition method. *Appl Math Mech Engl Ed* 2012; 33: 25–36.
11. Asadullah M, Khan U, Manzoor R, et al. MHD flow of a Jeffery fluid in a converging and diverging channels. *Int J Mod Math Sci* 2013; 6: 92–106.
12. Dib A, Haiahem A and Bou-said B. An analytical solution of the MHD Jeffery–Hamel flow by the modified Adomian decomposition method. *Comput Fluids* 2014; 102: 111–115.
13. Turkyilmazoglu M. Extending the traditional Jeffery-Hamel flow to stretchable convergent/divergent channels. *Comput Fluids* 2014; 100: 196–203.
14. Balmer RT and Kauzlaich JJ. Similarity solutions for the converging or diverging steady flow of non-Newtonian elastic power law fluids with wall suction or injection. Part I: two-dimensional channel flow. *AIChE J* 1971; 17: 1181–1188.
15. Forsyth TH. Converging flow of polymers. *Polym Plast Technol Eng* 1976; 6: 101–131.
16. Rajagopal KR, Gupta A and Vossoughi J. Slow flow of an incompressible third grade fluid in a converging/diverging channel. *J Technol* 1984; 28: 27–31.
17. Chakraborty AK and Metzner AB. Sink flows of viscoelastic fluids. *J Rheol* 1986; 30: 29–41.
18. Bhatnagar RK, Rajagopal KR and Gupta G. Flow of an Oldroyd-B fluid between intersecting planes. *J Non-Newton Fluid Mech* 1993; 46: 49–67.
19. Baris S. Flow of a second-grade visco-elastic fluid in a porous converging channel. *Turk J Eng Environ Sci* 2003; 27: 73–81.
20. Souza Mendes P and Sparrow EM. Periodically converging-diverging tubes and their turbulent heat transfer, pressure drop, fluid flow, and enhancement characteristics. *J Heat Transf* 1984; 106: 55–63.
21. Garg VK and Maji PK. Laminar flow and heat transfer in a periodically converging/diverging channel. *Int J Numer Methods Fluids* 1988; 8: 579–597.
22. Yilmaz T and Erdinc MT. *Fluid Flow Mixing for heat transfer enhancement in communicating converging and diverging channels*. ICHMT Digital Library Online Begel House Inc, 2014. DOI: 10.1615/ICHMT.2014.IntSympConvHeatMassTransf.630
23. Erdinc MT and Yilmaz T. Numerical Investigation of flow and heat transfer in communicating converging and diverging channels. *J Therm Eng* 2018; 4: 2318–2332.
24. Millsaps K and Pohlhausen K. Thermal distributions in Jeffery-Hamel flows between nonparallel plane walls. *J Aeronaut Sci* 1953; 20: 187–196.
25. Riley N. Heat transfer in Jeffery–Hamel flow. *Q J Mech Appl Math* 1989; 42: 203–211.
26. Mohyud-din ST, Khan U, Ahmed N, et al. Heat transfer analysis in diverging and converging channels. *Nonlinear Sci Lett A* 2012; 13: 61–71.
27. Khan U, Ahmed N, Zaidi ZA, et al. Effects of velocity slip and temperature jump on Jeffery Hamel flow with heat transfer. *Eng Sci Technol: Int. J* 2015. DOI: 10.1016/j.jestch.2014.09.001
28. Hayat T, Nawaz M, Sajid M, et al. The effect of thermal radiation on the flow of a second grade fluid. *Comput Math Appl* 2009; 58: 369–379.
29. Hayat T, Nawaz M and Sajid M. Effect of heat transfer on the flow of a second-grade fluid in divergent/convergent channel. *Int J Numer Methods Fluids* 2009; 64: 761–776.
30. RahimiPetroudi I, Ganji DD, Khazayi Nejad M, et al. Transverse magnetic field on Jeffery–Hamel problem with Cu–water nanofluid between two non parallel plane walls by using collocation method. *Case Stud Therm Eng* 2014; 4: 193–201.
31. Sheikholeslami M, Ganji DD and Ashorynejad HR. Investigation of squeezing unsteady nanofluid flow using ADM. *Powder Technol* 2013; 239: 259–265.
32. Dogonchi AS and Ganji DD. Investigation of MHD nanofluid flow and heat transfer in a stretching/shrinking convergent/divergent channel considering thermal radiation. *J Mol Liq* 2016; 220: 592–603.
33. Mohyud-Din ST, Khan U, Ahmed N, et al. A study of velocity and temperature slip effects on flow of water based nanofluids in converging and diverging channels. *Int J Appl Comput Math* 2015; 1: 569–587.
34. Schlichting H and Gersten K. *Boundary Layer Theory*. New York: Springer-Verlag, 2000.
35. Mansutti D and Ramgopal KR. Flow of a shear thinning fluid between intersecting planes. *Int J Non Linear Mech* 1991; 26: 769–775.
36. Mansutti D and Pontrelli G. Jefferey-Hamel flow of power-law fluids for exponent values close to the critical value. *Int J Non Linear Mech* 1991; 26: 761–767.
37. Rosenhead L. *Laminar boundary layers*. Clarendon: Dover, 1963.
38. Brewster ME, Chapman SJ, Fitt AD, et al. Asymptotics of slow flow of very small exponent power-law shear-thinning fluids in a wedge. *Eur J Appl Math* 1995; 6: 559–571.
39. Uribe FJ, Díaz-Herrera E, Bravo A, et al. On the stability of the Jeffery–Hamel flow. *Phys Fluids* 1997; 9: 2798–2800.
40. Harley C, Momoniat E and Rajagopal KR. Reversal of flow of a non-Newtonian fluid in an expanding channel. *Int J Nonlinear Mech* 2018; 101: 44–55.
41. Sochi T. Slip at fluid-solid interface. *Polym Rev* 2011; 51: 309–340.
42. Khan NA, Sultan F, Shaikh A, et al. Haar wavelet solution of the MHD Jeffery-Hamel flow and heat transfer in Eyring-Powell fluid. *AIP Adv* 2016; 6: 115102.
43. Puneeth V, Narayan SS, Manjunatha S, et al. Numerical simulation of Jeffrey–Hamel flow of nanofluid in the presence of gyrotactic microorganisms. *Int J Ambient Energy* 2021; 1–13. DOI: 10.1080/01430750.2021.1997812
44. Kumbinarasaiah S and Raghunatha KR. Numerical solution of the Jeffery–Hamel flow through the wavelet technique. *Heat Transf* 2022; 51: 1568–1584.

45. Ara A, Khan NA, Naz F, et al. Numerical simulation for Jeffery-Hamel flow and heat transfer of micropolar fluid based on differential evolution algorithm. *AIP Adv* 2018; 8: 015201.
46. Asghar Z, Saif RS and Ali N. Investigation of boundary stresses on MHD flow in a convergent/divergent channel: an analytical and numerical study. *Alex Eng J* 2022; 61: 4479–4490.
47. Mallikarjuna B, Rashad AM, Hussein AK, et al. Transpiration and thermophoresis effects on non-Darcy convective flow past a rotating cone with thermal radiation. *Arab J Sci Eng* 2016; 41: 4691–4700.
48. Bhuvaneswari M, Eswaramoorthi S, Sivasankaran S, et al. Cross-diffusion effects on MHD mixed convection over a stretching surface in a porous medium with chemical reaction and convective condition. *Engng Trans* 2019; 67: 3–19.
49. Ahmed SE, Mansour MA, Hussein AK, et al. Mixed convection from a discrete heat source in enclosures with two adjacent moving walls and filled with micropolar nanofluids. *Int J Eng Sci Technol* 2016; 19: 364–376.
50. Ahmed SE, Hussein AK, Mansour MA, et al. MHD mixed convection in trapezoidal enclosures filled with micropolar nanofluids. *Nanosci Techn Int J* 2018; 9: 343–372.
51. Ghachem K, Kolsi L, Mâatki C, et al. Numerical simulation of three-dimensional double diffusive free convection flow and irreversibility studies in a solar distiller. *Int Commun Heat Mass Transf* 2012; 39: 869–876.
52. Maatki C, Ghachem K, Kolsi L, et al. Inclination effects of magnetic field direction in 3D double-diffusive natural convection. *Appl Math Comput* 2016; 273: 178–189.
53. Pakdee W, Yuvakanit B and Hussein AK. Numerical analysis on the two-dimensional unsteady magnetohydrodynamic compressible flow through a porous medium. *J Appl Fluid Mech* 2017; 10: 1153–1159.
54. Elkhazen MI, Hassen W, Gannoun R, et al. Numerical study of electroconvection in a dielectric layer between two cofocal elliptical cylinders subjected to unipolar injection. *J Eng Phys Thermophys* 2019; 92: 1318–1329.
55. Kasmani R, Sivasankaran S, Bhuvaneswari M, et al. Analytical and numerical study on convection of nanofluid past a moving wedge with Soret and Dufour effects. *Int J Numer Method Heat Fluid Flow* 2017; 27: 2333–2354.
56. Tsai R and Huang JS. Heat and mass transfer for Soret and Dufour's effects on Hiemenz flow through porous medium onto a stretching surface. *Int J Heat Mass Transf* 2009; 52: 2399–2406.
57. Makinde OD and Olanrewaju PO. Unsteady mixed convection with Soret and Dufour effects past a porous plate moving through a binary mixture of chemically reacting fluid. *Chem Eng Commun* 2011; 198: 920–938.
58. Kumar P and Mei San S. CFD study of the effect of venturi convergent and divergent angles on low pressure wet gas metering. *J Appl Sci* 2014; 14: 3036–3045.
59. Taha ES, Abdulwahid MA, Morad AMA, et al. Computational fluid dynamic analysis of the flow through T-junction and venturi meter. In: *IMDC-IST*, 2022. EAI.
60. Barrios-Piña H, Ramírez-León H and Couder-Castañeda C. Analysis of flow evolution and thermal instabilities in the near-nozzle region of a free plane laminar jet. *Math Probs Eng* 2015; 2015: 1–11.
61. Hu P, Wang P, Liu L, et al. Numerical investigation of Tesla valves with a variable angle. *Phys Fluids* 2022; 34: 033603.

Appendix

This section comprises of details regarding derivation of equations (8)(10) from governing equations (2)–(5) by the use of transformations, equations (6) and (7). First of all eliminate the pressure gradient terms between equations (3) and (4), then we have

$$\frac{\partial}{\partial\theta}\left(u\frac{\partial u}{\partial r}\right) = -2\nu\frac{\partial}{\partial r}\left(\frac{1}{r}\frac{\partial u}{\partial\theta}\right) + \nu\frac{\partial}{\partial\theta}\left(\frac{\partial^2 u}{\partial r^2} + \frac{1}{r}\frac{\partial u}{\partial r} + \frac{1}{r^2}\frac{\partial^2 u}{\partial\theta^2} - \frac{u}{r^2}\right),$$

Which after expansion gets the form

$$\frac{\partial u}{\partial\theta}\frac{\partial u}{\partial r} + u\frac{\partial^2 u}{\partial\theta\partial r} = \frac{2\nu}{r^2}\frac{\partial u}{\partial\theta} - \frac{2\nu}{r}\frac{\partial^2 u}{\partial\theta\partial r} + \nu\left(\frac{\partial^3 u}{\partial\theta\partial r^2} + \frac{1}{r}\frac{\partial^2 u}{\partial\theta\partial r} + \frac{1}{r^2}\frac{\partial^3 u}{\partial\theta^3} - \frac{1}{r^2}\frac{\partial u}{\partial\theta}\right).$$

We now make use of equation (6) in last equation, that results into

$$-\frac{1}{r^3}ff' - \frac{1}{r^3}ff' = \frac{2\nu}{r^3}f' + \frac{2\nu}{r^3}f' + \nu\left(\frac{2}{r^3}f' + \frac{1}{r^3}f' + \frac{1}{r^3}f''' - \frac{1}{r^3}f'\right).$$

Some further simplification yields the following

$$f'''(\theta) + 4\nu f'(\theta) + 2f(\theta)f'(\theta) = 0.$$

In view of equation (7) ($F(\eta) = f(\theta)/U$ and $\eta = \theta/\alpha$), the above equation becomes (Equation (8))

$$F'''(\eta) + 2\mathrm{Re}\alpha F(\eta)F'(\eta) + 4\alpha^2 F'(\eta) = 0, \quad \text{with } \mathrm{Re} = U\alpha/\nu.$$

Now we consider energy equation, equation (4), which in the light of equation (7) becomes

$$-2\rho c_p T_w\frac{UF(\eta)\beta(\eta)}{r^4} = k\left(\frac{6T_w\beta(\eta)}{r^4} - \frac{2T_w\beta(\eta)}{r^4} + \frac{T_w\beta''(\eta)}{\alpha^2 r^4}\right) + \mu\left(2\left(\frac{U^2F^2(\eta)}{r^4} + \frac{U^2F^2(\eta)}{r^4}\right) + \frac{U^2(F'(\eta))^2}{\alpha^2 r^4}\right) + \frac{DK_T}{C_s}\left(\frac{6C_w\phi(\eta)}{r^4} - \frac{2C_w\phi(\eta)}{r^4} + \frac{C_w\phi''(\eta)}{\alpha^2 r^4}\right).$$

The simplification leads to the following

$$\frac{k}{\mu c_p}(\beta''(\eta)+4\alpha^2\beta(\eta))+\frac{U^2}{T_w c_p}\left(4\alpha^2F^2(\eta)+(F'(\eta))^2\right)$$
$$+2\alpha\left(\frac{U\alpha}{\nu}\right)\beta(\eta)F(\eta)+\frac{DK_TC_w}{C_s\mu c_pT_w}(4\alpha^2\phi(\eta)+\phi''(\eta))=0.$$

The introduction of the nondimensional numbers

$$\mathrm{Re}=\frac{U\alpha}{\nu},\ \mathrm{Pr}=\frac{\mu c_p}{k},\ Ec=\frac{U^2}{c_pT_w},\ D_f=\frac{DK_TC_w}{C_s\mu c_pT_w},$$

reduce the last equation into

$$\frac{1}{\mathrm{Pr}}(\beta''(\eta)+4\alpha^2\beta(\eta))+Ec\left(4\alpha^2F^2(\eta)+(F'(\eta))^2\right)$$
$$+2\mathrm{Re}\alpha\beta(\eta)F(\eta)+D_f(4\alpha^2\phi(\eta)+\phi''(\eta))=0.$$

This can further be written as

$$\beta''(\eta)+2\alpha^2\left(2+\frac{\mathrm{Pr}\,Re}{\alpha}F(\eta)\right)\beta(\eta)$$
$$+\mathrm{Pr}\,Ec\left(4\alpha^2F^2(\eta)+(F'(\eta))^2\right)$$
$$+\mathrm{Pr}\,D_f(4\alpha^2\phi(\eta)+\phi''(\eta))=0,$$

which by invoking $\mathrm{Pr}\,Re=Pe$, $\mathrm{Pr}\,Ec=Br$ gets the form of equation (9) as

$$\beta''(\eta)+2\alpha^2\left(2+\frac{Pe}{\alpha}F(\eta)\right)\beta(\eta)+Br\left(4\alpha^2F^2(\eta)+(F'(\eta))^2\right)$$
$$+\mathrm{Pr}\,D_f(4\alpha^2\phi(\eta)+\phi''(\eta))=0.$$

Now come to the mass transport equation, equation (5) which in view of equations (6) and (7) get the following form

$$\frac{UF(\eta)}{r}\frac{\partial}{\partial r}\left(\frac{C_w\phi(\eta)}{r^2}\right)$$
$$=D\left(\frac{\partial^2}{\partial r^2}\left(\frac{C_w\phi(\eta)}{r^2}\right)+\frac{1}{r}\frac{\partial}{\partial r}\left(\frac{C_w\phi(\eta)}{r^2}\right)\right.$$
$$\left.+\frac{1}{r^2\alpha^2}\frac{\partial}{\partial\eta^2}\left(\frac{C_w\phi(\eta)}{r^2}\right)\right)+\frac{DK_T}{T_m}\left(\frac{\partial^2}{\partial r^2}\left(\frac{T_w\beta(\eta)}{r^2}\right)\right.$$
$$\left.+\frac{1}{r}\frac{\partial}{\partial r}\left(\frac{T_w\beta(\eta)}{r^2}\right)+\frac{1}{r^2\alpha^2}\frac{\partial}{\partial\eta^2}\left(\frac{T_w\beta(\eta)}{r^2}\right)\right).$$

The simple algebra on the above equation gives

$$-2\left(\frac{U\alpha}{\upsilon}\right)\alpha F(\eta)\phi(\eta)=\frac{D}{\nu}(4\alpha^2\phi(\eta)+\phi''(\eta))$$
$$+\frac{DT_wK_T}{T_m\nu C_w}(\beta''(\eta)+4\alpha^2\beta(\eta)).$$

The use of dimensionless numbers,

$$\mathrm{Re}=\frac{U\alpha}{\nu},\quad S_c=\frac{\nu}{D},\quad S_r=\frac{DT_wK_T}{T_m\nu C_w},$$

into last equation yields the following form of mass transport equation,

$$\frac{1}{S_c}(\phi''(\eta)+4\alpha^2\phi(\eta))+S_r(\beta''(\eta)+4\alpha^2\beta(\eta))$$
$$+2Re\alpha F(\eta)\phi(\eta)=0.$$

The more rearrangement of this equation gives equation (10)

$$\phi''(\eta)+2\alpha^2\left(2+\frac{ReSc}{\alpha}F(\eta)\right)\phi(\eta)$$
$$+S_rS_c(\beta''(\eta)+4\alpha^2\beta(\eta))=0.$$

Notation

$u=u(r,\theta)$	Radial component of velocity
(r,θ)	Polar coordinates
c_p	Specific heat
k	Thermal conductivity
K_T	Thermal diffusion ratio
$C=C(r,\theta)$	Concentration
T_m	Mean fluid temperature
ρ	Density
μ	Dynamic viscosity
$\phi(\eta)$	Dimensionless concentration
Re	Reynolds number
Pr	Prandtl number
D_f	Dufour number
Sr	Soret number
q	Constant volume flow rate
∇	Gradient vector
$\mathbf{t}$	Traction vector
n_r, n_θ, n_z	Components of Normal **n**
$\tilde{r}$	specific value of r
tr	Traction parameter
O	Outflow
$\mathbb{R}^+$	Set of positive real numbers
HAM	Homotopy Analysis Method
ADM	Adomian Decomposition Method
HWM	Hermite wavelet method
C_w	Concentration at the wall
$v=v(r,\theta)$	Transverse velocity
$p=p(r,\theta)$	Pressure
$T=T(r,\theta)$	Temperature
D	Mass diffusivity
C_s	Concentration susceptibility
K_1	Chemical reaction
$F(\eta)$	Dimensionless Velocity
ν	Kinematic viscosity
$\beta(\eta)$	Dimensionless temperature
η	Dimensionless angle
α	Angle between walls

Ec	Eckert number	$\mathbf{I}$	Inflow
Sc	Schmidt number	tr	Radial direction force
$\mathbf{T}$	Cauchy stress tensor	$\mathbb{R}^-$	Set of negative real numbers
$\mathbf{I}$	Identity tensor	RK	Runge-Kutta
$\mathbf{V}$	Velocity vector	DRA	Daun-Rach Approach
$\mathbf{n}$	Unit normal to the surface	T_w	Temperature at the wall
$\mathbf{t}_r, \mathbf{t}_\theta, \mathbf{t}_z$	Traction vector components	$y_k, k = 1, 2, \cdots, 6$	Variables for order reduction
$u_i, i = 1, 2, \cdots, 5$	Initial guess		